Fabrication and Mechanical Properties of Textured Ti_3SiC_2 by Slip Casting in a Strong Magnetic Field Followed by Spark Plasma Sintering

Yoshio SAKKA[1*], Kimitoshi SATO[1], Hiroto HIRANO[1, 2], Takamasa ISHIGAKI[2], Tohru S. SUZUKI[1] and Koji MORITA[1]

[1] National Institute for Materials Science, 1-2-1 Sengen, Tsukuba, Ibaraki, 305-0047, Japan
[2] Hosei University, 3-7-2 Kajino-cho, koganei, Tokyo, 184-8584, Japan

Abstract
Ti_3SiC_2 with a nacre-like microstructure was fabricated by slip casting in a strong magnetic field followed by spark plasma sintering (SPS). To determine the effect of the grain size and texture on the mechanical properties, two textured and non-textured Ti_3SiC_2 ceramics with different grain sizes were prepared with the different initial particle size and SPS sintering temperature. A powder with relatively large plate-like Ti_3SiC_2 particles was fabricated by the templated-grain growth method. Increasing the grain size increased the fracture toughness of the textured Ti_3SiC_2 ceramics but decreased the three-point bending strength. The three-point bending strength and fracture toughness of the textured Ti_3SiC_2 with the large grain size were 812 MPa and 7.3 MPa・$m^{1/2}$, and those with the small grain size were 1045 MPa and 5.6 MPa・$m^{1/2}$, respectively. Furthermore, catastrophic failure of the textured Ti_3SiC_2 ceramics after the fracture toughness test was prevented, similarly to in fiber-reinforced ceramics.

Keywords: MAX phase ceramics, colloidal processing, textured ceramics, mechanical property, SPS

Introduction

Natural nacre possesses a layered microstructure with alternating soft and tough layers, which gives it excellent compressive and tensile properties.[1)] Many material scientists have attempted to simulate the laminar configuration of nacre, with the aim of improving the mechanical properties of inorganic ceramics.[2, 3)] They found that crack deflection and the subsequent growth of delamination cracks were the source of energy dissipation during the fracture of layered ceramics, which contributed to the marked enhancement of the work of fracture. MAX-phase ceramics is the general term for layered compounds represented by $M_{n+1}AX_n$ (where n is 1, 2 or 3, M is a pre-period transition metal, A is a group A element and X is C or N). A nacre-like microstructure can be assembled using MAX phases, to have their specific nanolayered crystal structure with strong M-X bonds and weak M-A bonds.[4)] To assemble such a nacre-like microstructure, the fabrication of a textured MAX-phase ceramic is required. Colloidal processes, such as slip casting,[5-8)] gel casting [9)] and electrophoretic deposition,[10)] in a strong magnetic field have been successfully conducted to obtain textured MAX-phase ceramics using the anisotropic magnetic susceptibility of MAX phases owing to the anisotropic crystal structure.[11)] Several textured MAX phase ceramics with high strength and fracture toughness have been reported. [6), 12)]

Ti_3SiC_2 in the MAX phase is most commonly studied. Hu et al. attempted to fabricate textured Ti_3SiC_2 ceramics in the same way, but their mechanical properties, such as strength and fracture toughness, were not measured because the powder started to decompose at approximately 1000 °C.[8)] Barsoum et al. argued that the reduced temperature at which Ti_3SiC_2 decomposed was due to the presence of impurity phases in the starting powders.[13)] Almost reported data have been prepared by pressure sintering such as hot press, SPS, etc. We have succeeded in fabrication of dense Ti_3SiC_2 ceramics by pressureless sintering using sinterable powder. The strength of the resulting oriented ceramics was higher than that of the reported pressure-sintered samples, but the fracture toughness was smaller. To achieve high fracture toughness via crack deflection and the pull-out of plate-like particles, grain growth in textured Ti_3SiC_2 sintered samples using relatively large particles fabricated by templated-grain growth[14)] should be effective. In this study, two types of powders with different particle sizes were prepared, compacted in a magnetic field, and then SPS sintered to obtain samples with different grain sizes, and their strength and toughness were investigated.

Experimental Procedure

Powders of Ti (TIE07P13, Kojundo Chemical Laboratory Co., Ltd., Saitama, Japan), Si (No.600, Yamaishi Metal Co., Ltd., Chiba, Japan), TiC (TI-30-10-0020, RARE METALLIC Co., Ltd., Tokyo, Japan) and Al (ALE15PB, Kojundo Chemical Laboratory Co., Ltd.) were used as starting powders. These powders were ball-milled with a molar ratio of 1.0 Ti: 1.2 Si: 0.3 Al: 2.0 TiC using ϕ 5 mm ZrO_2 balls for 24 h in ethanol. Al was added for deoxygenation of the reacting powders,[15)] and Si was added in an excess of the stoichiometric amount to increase the contact area between Si and Ti.[16, 17)] After drying, the powder mixture was placed in an alumina crucible and heated in a tungsten heating furnace (NM-15, New Equipment Machinery System Ltd., Fukushima, Japan) in Ar at 1200 °C for 2 h at a heating rate of 20 °C/min. The aggregated powder was deaggregated using an alumina mortar and had a mean particle size of 2.5 μm. This fine powder is used for fabricating fine grained Ti_3SiC_2 and also for preparing large powders. Our

*corresponding author, E-mail: sakka.yoshio@nims.go.jp

previous experiment showed that Ti_3SiC_2 powder with relatively large particles cannot be obtained by simply increasing the synthesis temperature to, for example, 1300 or 1400° C. Therefore, using the fine powder, relatively large particles were fabricated by the following templated-grain growth method [14), 18)]. The fine powder was mixed with the starting raw powders having a molar ratio of 1.0 Ti: 1.2 Si: 0.3 Al: 2.0 TiC in ethanol at a weight ratio of 5:5. After drying, the powder mixture was placed in an alumina crucible and heated in a tungsten furnace in Ar at 1400 °C for 2 h at a heating rate of 20 °C/min. The aggregated powder was deaggregated and the layered samples were exfoliated by ball milling with ϕ 10 mm ZrO_2 balls for 24 h in ethanol.

Phase analysis of the synthesized powders was carried out by X-ray diffraction (XRD) using a diffractometer equipped with a CuK α source (RINT2500, Rigaku Co., Ltd., Tokyo, Japan). The morphology was examined by scanning electron microscopy (SEM) and the particle size distribution was determined by image analysis as follows. The primary particle sizes of 1000 synthesized particles were measured and the cumulative volume curve was drawn by assuming that all particles were spherical. The median diameter D_{50} was assumed to be the mean diameter.

An ethanol suspension with 25 vol% solid loading was prepared and used for slip casting. Polyethylenimine (PEI) with an average molecular weight of 10,000 and polyvinyl butyral (PVB) with an average molecular weight of 100,000 were added as a polymer dispersant and binder, respectively. The amounts of added PEI and PVB were 1.0 and 1.0 wt%, respectively. To obtain textured Ti_3SiC_2 ceramics, the suspension was slipcast in a 12 T magnetic field applied in the horizontal direction. The stage used in slip casting was rotated at 20 rpm to rotate the magnetic field,[19, 20)] since the magnitudes of magnetic susceptibility along the a- and b-axes are larger than that along the c-axis in the Ti_3SiC_2 system.[8)] To obtain a dense sample, the green body was subjected to cold isostatic pressing under a pressure of 392 MPa for 10 min, which was followed by sintering in an SPS apparatus (100 kNSPS-1050, Syntex Inc., Kanagawa, Japan) in flowing argon.[21)] To remove organic materials, the samples were also heated to 650 °C for 1 h under a reduced pressure of 10^{-1} Pa with the Ar gas replaced when the temperature reached 650 °C. The sintering temperature was set to 1200°C for fine powder and 1450 °C for large powder with a heating rate of 50 °C/min and the sintering temperature was maintained for 10 min. A uniaxial pressure of 80 MPa was applied parallel to the slip-casting direction.

The degree of orientation, L_f, was estimated using the Lotgering orientation factor, defined as

$$L_f = (P-P_0) / (1-P_0), \quad (1)$$

where

$$P = [\Sigma I(00l) / \Sigma I(hkl)] \quad (2)$$

and P_0 represents the same quantity for a nonoriented sample. L_f varies from zero for a nonoriented sample to one for a completely oriented sample. In this study, P_0 was calculated from the peak data of JCPDS card No.74-0310.

Bars with dimensions of 2×1.5×18 mm were cut from the sintered samples, and their fracture strength was measured by performing three-point fracture strength tests with the span size set at 16 mm and a crosshead speed of 0.5 mm/min. The average bending strength was obtained from measurements of five samples. To measure the fracture toughness, 4×2×18 mm bars were also cut, and a V-shaped notch with a depth of 0.5 mm and an end curvature radius of 10 μm was formed at the center of the specimen. Then fracture toughness tests were carried out with the span size set at 16 mm and a crosshead speed of 0.05 mm/min. The fracture toughness was calculated from the obtained results using the equation proposed by Wakai et al.[22)] The average fracture toughness was obtained from measurements of five samples.

Fractured surfaces of the sintered samples were characterized by SEM (TM3000, Hitachi Miniscope, Hitachi Ltd., Tokyo, Japan). Sintered samples etched by an acid solution of H_2O, HNO_3 and HF with a volume ratio of 1:1:1 were observed by SEM. The mean grain size and thickness were determined by the measurement of 200 grains by image analysis.

Results and Discussion

Fig. 1 shows the particle size distributions of the fine and relatively large Ti_3SiC_2 powders, where the latter comprises a mixture of the fine Ti_3SiC_2 powder and the raw powders in the starting mixture, heated at 1300 and 1400 °C for 2 h. The particle size gradually

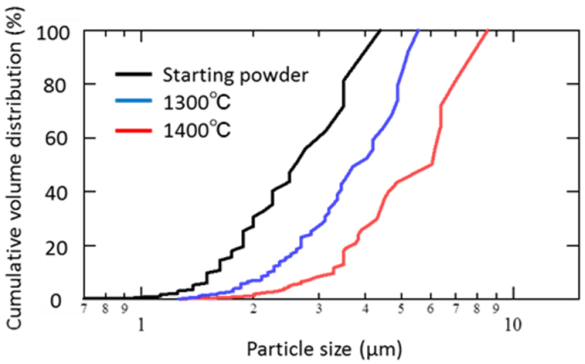

Fig. 1 Particle size distributions of the fine and relatively large Ti_3SiC_2 powders, where the latter comprises a mixture of the fine Ti_3SiC_2 powder and the raw powders in the starting mixture, heated at 1300 and 1400 °C for 2 h.

increased with increasing temperature. The mean particle size of the Ti_3SiC_2 powder heated at 1300 °C for 2 h was approximately 3.5 μm. The particle size of the powder heated at 1400 °C for 2 h ranged from 1 to 10 μm and the mean particle size was approximately 6 μm. The growth rate on the (002) plane was lower than those on the (100) and (101) planes.[23] The starting raw mixture powders in the neighborhood of the (100) and (101) planes should promote grain growth. Fig. 2 shows XRD profiles of the Ti_3SiC_2 powders with relatively large particles heated at 1300 and 1400 °C for 2 h. Almost single-phase Ti_3SiC_2 was observed in these powders.

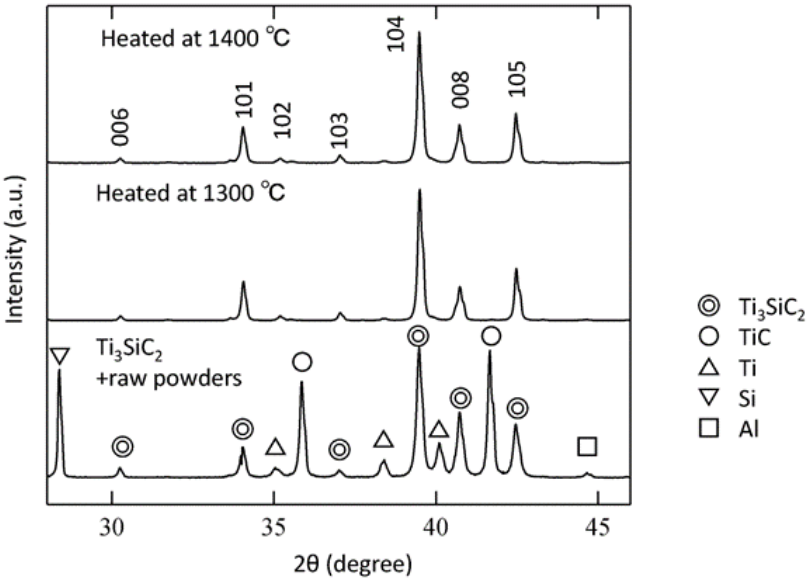

Fig. 2 XRD profiles of the Ti_3SiC_2 powders heated at 1300 or 1400 °C for 2 h. Mixtures of fine Ti_3SiC_2 powder of 2.5 mm and the starting raw powder with a weight ratio of 5:5 was heated at 1300 or 1400 °C.

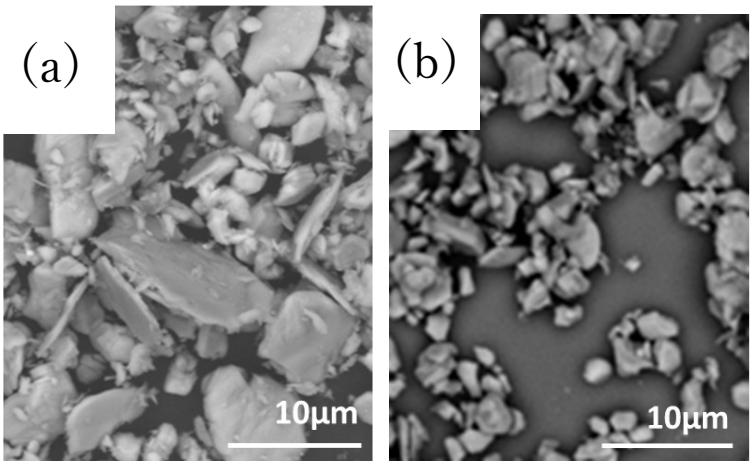

Fig. 3 SEM images of the ball-milled Ti_3SiC_2 powder with relatively large particles heated at 1400 °C (a) and the ball-milled starting Ti_3SiC_2 powder (b).

Fig. 3 shows SEM images of the initial fine powder and ball-milled powder with relatively large particles heated at 1400 °C for 2 h. Both powders appeared to be deagglomerated. The fine powder had a particle size of 1 to 4 μm. In contrast, the large Ti_3SiC_2 powder heated at 1400 °C for 2 h had a particle size of 1 to 10 μm and contained a mixture of relatively large plate-like and small particles.

Using the fine powder, a textured Ti_3SiC_2 ceramic was fabricated by slip casting in a strong magnetic field followed by SPS at 1200 °C for 10 min under a pressure of 80 MPa. An almost non-textured (hereafter denoted as non-textured) Ti_3SiC_2 ceramic was also fabricated by slip casting without a magnetic field followed by SPS at 1200 °C for 10 min under a pressure of 80 MPa. The relative densities of the textured and non-textured Ti_3SiC_2 ceramics were 99.7% and 98.9%, respectively. The calculated Lotgering orientation factors were $L_f(00l) = 0.62$ for the textured top surface of the sintered sample and $L_f(00l) = 0.01$ for the nontextured top surface of the sintered sample. The mean grain size of the both the textured and nontextured Ti_3SiC_2 ceramics was approximately 2.5 μm, the same as that of the powder synthesized at 1200 °C for 2 h.

In the samples prepared by slip casting of the large powder in a magnetic field followed by SPS, the relative density of the samples

sintered at 1450°C for 10 min under a pressure of 80 MPa was 97.8%. In the samples prepared by slip casting without a magnetic field, the relative density sintered at the same conditions was 98.1 %.

Fig. 4 shows XRD patterns of the textured top (a) and side (b) surfaces of the Ti_3SiC_2 ceramics prepared using the large powder. On the textured side surface, the (101), (104) and (110) planes exhibit the three strongest diffraction peaks, whereas on the textured top surface, only (00l) planes exist. The Lotgering orientation factors were calculated to be L_f (001) = 0.94 on the textured top surface of the sample sintered at 1450 °C for 10 min. In contrast, the Lotgering orientation factors were calculated to be L_f (00l) = 0.16 on the non-textured top surface of the samples sintered at 1450 °C for 10 min.

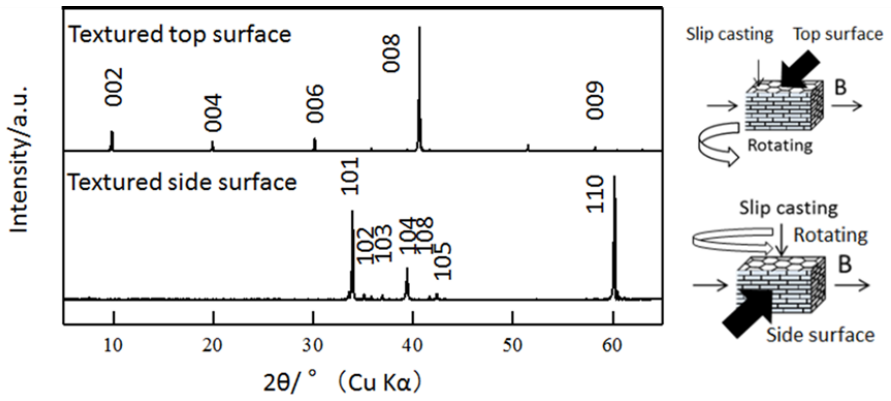

Fig. 4 XRD patterns of the textured top (a) and side (b) surfaces of Ti_3SiC_2 ceramics prepared by slip cast in a strong magnetic field followed by SPS at 1450 °C for 2 h.

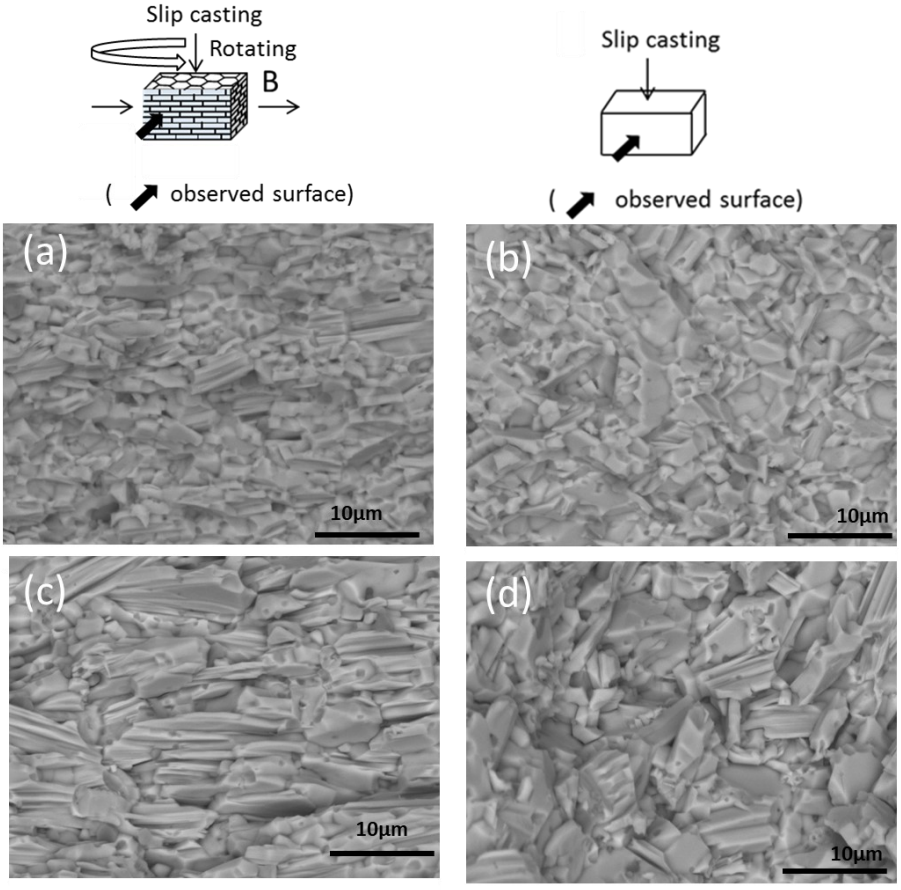

Fig. 5 SEM images of the fractured side surface of textured samples sintered at 1200 (a) and 1450 °C (c) prepared by slip cast in a strong magnetic field followed by SPS, respectively. SEM images of the surface perpendicular to the slip-casting direction of the samples sintered at 1200 (b) and 1450 °C (d) prepared by slip cast without a magnetic field followed by SPS, respectively. All fractured surfaces were observed from the direction perpendicular to the slip-casting direction.

Figs. 5 (a) and (c) show SEM images of the fractured side surface of the textured samples subjected to SPS at 1200 and 1450 °C, respectively. Figs. 5 (b) and (d) show SEM images of the fractured surface of the non-textured samples SPS sintered at 1200 and

1450 °C. For the samples prepared by slip casting in a magnetic field followed by SPS, the c-axis of the plate-like Ti_3SiC_2 grains was oriented parallel to the slip-casting direction, as shown in Fig. 5.

Table 1 summarizes the grain size, three-point bending strength and fracture toughness of the sintered samples. For oriented samples, grain size is indicated by the grain size on the top (c-plane) and the side is indicated by the thickness. The grain size increased with the sintering temperature, regardless of the texturing of the samples.

Table 1 Grain size [thickness], three-point bending strength and fracture toughness of the sintered Ti_3SiC_2 samples.

Sample	Grain size [Thichness] (μm)	3 point bending strength (MPa)	Fracture toughness (MPa・$m^{1/2}$)
Textured			
Sintered at 1200°C	2.5 [1.0]	1045±75	5.6±0.1
Sintered at 1450°C	10.0 [1.9]	812±50	7.3±0.4
Without magnetic field			
Sintered at 1200°C	2.5	860±45	5.8±0.1
Sintered at 1450°C	6.0	772±5	6.0±0.1

When the grain size of the textured Ti_3SiC_2 ceramic was the same as that of the fine powder, the fracture toughness of the textured Ti_3SiC_2 sintered sample was almost the same as that of the non-textured Ti_3SiC_2 sintered sample, despite the increased three-point bending strength. The crack deflection and pull-out of the textured Ti_3SiC_2 sintered samples do not appear to be effective when the grain size is small.

The fracture toughness of the two non-textured samples was almost the same. In contrast, in the textured samples, the fracture toughness was markedly higher. Compared with the non-textured sample sintered at 1450 °C, the three-point bending strength and fracture toughness of the textured sample sintered under the same conditions were increased by factors of 1.22. Fig. 6 shows SEM images of (a) the textured and (b) non-textured test specimens sintered at 1450 °C after K_{1C} measurement. It can be seen that the

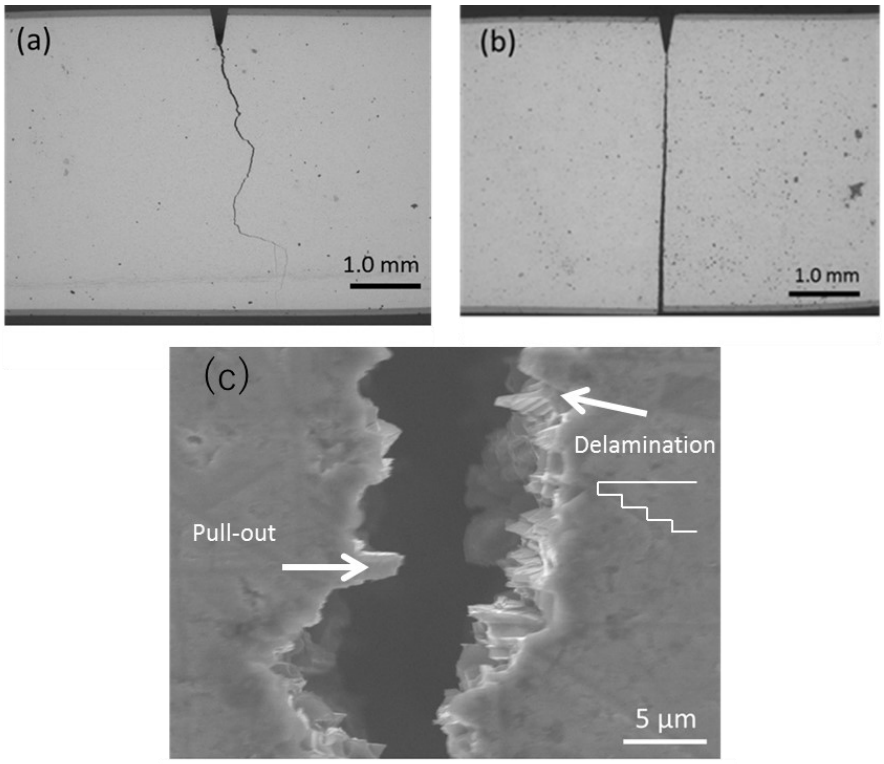

Fig. 6 Crack propagation behavior after K1C measurement by single-edge V-notched beam method for the textured sample (a) and almost nontextured sample (b). Pull-out of the plate-like grains and delamination of the layered Ti_3SiC_2 particles during crack propagation.(c).

crack propagation of the textured Ti_3SiC_2 ceramics is different from that of the nontextured Ti_3SiC_2 ceramics. A crack in the textured Ti_3SiC_2 ceramics propagates in a zigzag manner. Fig. 6(c) shows magnified SEM images of Fig. 6 (a). The pull-out of the plate-like grains and the delamination of layered Ti_3SiC_2 particles can be seen. The higher fracture toughness and strength of the textured Ti_3SiC_2 ceramics sintered at 1450 °C are attributed to the enhanced pull-out and delamination of the plate-like particles and crack deflection. After the K_{1C} measurement of the textured sample, the sample retained its integral shape without catastrophic failure as shown in Fig. 6 (a). Kagawa et al. fabricated $MgAl_2O_4$ reinforced with SiC fibers.[24)] The fibers were aligned unidirectionally in the matrix. Although the fracture toughness of the monolithic $MgAl_2O_4$ could not be improved, its catastrophic failure was prevented by the bridging effect of the fibers. In our textured Ti_3SiC_2 ceramics, catastrophic failure was similarly prevented but further research is necessary to clarify the mechanism preventing catastrophic failure. Also more systematic studies are required to clarify the effect of grain size on the fracture toughness.

Conclusion

Textured Ti_3SiC_2 ceramics with different grain sized were fabricated by slip casting in a strong magnetic field followed by SPS at 1200 and 1450 °C under a pressure of 80 MPa for 10 min. To achieve high fracture toughness via crack deflection and the pull-out of plate-like Ti_3SiC_2 particles, grain growth in the textured Ti_3SiC_2 sintered samples was considered to be effective. Therefore, powders with relatively large plate-like Ti_3SiC_2 particles were fabricated by templated-grain growth and used as textured Ti_3SiC_2 ceramics. The Lotgering orientation factor of the textured Ti_3SiC_2 ceramics was 0.97. The three-point bending strength and fracture toughness of the textured Ti_3SiC_2 ceramics, obtained by the single-edge V-notched beam method, were 812 MPa and 7.3 MPa・$m^{1/2}$, respectively. Furthermore, catastrophic failure of the textured Ti_3SiC_2 after the fracture toughness test was prevented, similarly to in fiber-reinforced ceramics. These mechanical properties were attributed to pull-out and delamination of the plate-like particles and crack deflection.

Acknowledgments

This work was partially supported by Grant-in-Aid for Scientific Research B No.23350104 and No.20H02444 from Japan Society for the Promotion of Science.

References

1) A. Y. M. Lin, M. A. Meyers, K. S. Vecchio: Mater. Sci. Eng., **C26** (2006) 1380-1389.
2) D. Kovar, M. D. Thouless, J. W. Halloran: J. Am. Ceram. Soc., **81** (1998) 1004-1012.
3) E. Munch, M. E. Launey, D. H. Alsem, E. Saiz, A. P. Tomsia, R. O. Ritchie: Science, **322** (2008) 1516-1520.
4) Z. M. Sun: Inter. Mater. Rev. , **56** (2011) 143-166.
5) C. Hu, Y. Sakka, T. Nishimura, S. Guo, S. Grasso, H. Tanaka: Sci. Technol. Adv. Mater., **12** (2011) 04460 .
6) C. Hu, Y. Sakka, S. Grasso, T. Nishimura, S. Guo, H. Tanaka: Scr. Mater., **64** (2011) 765-768.
7) C. Hu, Y. Sakka, H. Tanaka, T. Nishimura, S. Grasso: J. Am. Ceram. Soc., **94** (2011) 410-415.
8) C. Hu, Y. Sakka, S. Grasso, T. Suzuki, H. Tanaka: J. Am. Ceram. Soc., **94** (2011) 742-748.
9) M. Mishra, Y. Sakka, A. Szudarska, M. Szafran, T. S. Suzuki, T. Uchikoshi : J. Ceram. Soc. Jpn., **120** (2012) 544-547.
10) M. Mishra, Y. Sakka, C. F. Hu, T.S. Suzuki, T. Uchikoshi, L. Besra: J. Am. Ceram. Soc., **95** (2012) 2857–2862.
11) Y. Sakka, T. S. Suzuki: J. Ceram. Soc. Jpn., **113** (2005) 26–36.
12) Y. Sakka: KONA Powder Particle J., **36** (2019) 114-128.
13) N. Tzenov, M. W. Barsoum, T. EI-Raghy: J. Eur. Ceram. Soc., **20** (2000) 801-806.
14) M. Seabaugh, G. Cheney, K. Hasinska, A. Azad, E. Sabolsky, S. Swartz, W. Dawson: J. Intelligent Mater. System and Structure, **15** (2004) 209-214.
15) Y. Zhou, Z. M. Sun, S. Tada, H. Hashimoto: J. Alloys Comp., **461** (2008) 579-584.
16) K. Sato, M. Mishra, H. Hirano, C. Hu, Y. Sakka: J. Am. Ceram. Soc., **97** (2014) 1407-1412.
17) K. Sato, M. Mishra, H. Hirano, T. S. Suzuki, Y. Sakka: J. Ceram. Soc., Jpn., **122** (2014) 817-812.
18) K. Sato, H. Hirano, T. S. Suzuki, T. Ishigaki, Y. Sakka: J. Soc. Powder Tech. Jpn., **51** (2014) 163-168 [in Japanese].
19) S. Tanaka, A. Makiya, Z. Kato, N. Uchida, T. Kimura, K. Uematsu: J. Mater. Res., **21** (2006) 703-707.
20) X. W. Zhu, Y. Sakka, T. S. Suzuki, T. Uchikoshi, S. Kikkawa: Acta. Mater., **58** (2010) 146-161.
21) S. Grasso, Y. Sakka, G. Maizza: Sci. Technol.Adv. Mater., **10** (2009) 053001.
22) F. Wakai, S. Sakaguchi, Y. Matsuno: Yogyo-Kyokai-Shi, **93** (1985) 479-480 [in Japanese].
23) Y. Zhou, Z. Sun,: J. Mater.Sci., **35** (2000) 4343-4346 .
24) A. F. Dericioglu, Y. Kagawa: J. Mater. Sci., **37** (2002) 523–530.